ISSN 0021-8944, Journal of Applied Mechanics and Technical Physics, 2017, Vol. 58, No. 1, pp. 116–128. © Pleiades Publishing, Ltd., 2017.
Original Russian Text © N. Samyuktha, R. Ravindran, M. Ganapathirao.

# EFFECTS OF THE CHEMICAL REACTION AND HEAT GENERATION OR ABSORPTION ON A MIXED CONVECTION BOUNDARY LAYER FLOW OVER A VERTICAL STRETCHING SHEET WITH NONUNIFORM SLOT MASS TRANSFER

**N. Samyuktha[a], R. Ravindran[a†], and M. Ganapathirao[b]**

UDC 536.3

**Abstract:** An analysis is performed to study the effects of the chemical reaction and heat generation or absorption on a steady mixed convection boundary layer flow over a vertical stretching sheet with nonuniform slot mass transfer. The governing boundary layer equations with boundary conditions are transformed into the dimensionless form by a group of nonsimilar transformations. Nonsimilar solutions are obtained numerically by solving the coupled nonlinear partial differential equations using the quasi-linearization technique combined with an implicit finite difference scheme. The numerical computations are carried out for different values of dimensionless parameters to display the distributions of the velocity, temperature, concentration, local skin friction coefficient, local Nusselt number, and local Sherwood number. The results obtained indicate that the local Nusselt and Sherwood numbers increase with nonuniform slot suction, but nonuniform slot injection produces the opposite effect. The local Nusselt number decreases with heat generation and increases with heat absorption.

*Keywords:* nonuniform slot suction, mixed convection, stretching sheet, chemical reaction, heat generation.

**DOI:** 10.1134/S0021894417010138

## INTRODUCTION

The boundary layer on a continuously moving surface has many applications in manufacturing industries and technological processes, such as glass-fibre production, wire drawing, paper production, tinning of copper wires, production of coaxial television cables, metal and polymer processing industries, etc.

A pioneering study of the boundary layer flow on a continuously moving surface was performed by Sakiadis [1]. Tsou et al. [2] showed experimentally that such a flow is physically realizable and explored its basic characteristics. Erickson et al. [3] extended the work of Sakiadis [1] to include blowing or suction at the flat plate surface. Crane [4] investigated the flow past a stretching plate with a constant temperature. Gupta and Gupta [5] analyzed the stretching sheet problem with a constant surface temperature in the presence of suction or blowing, while Soundalgekar and Murty [6] investigated a constant surface velocity with power-law temperature variation.

[†]Deceased.

[a]Department of Mathematics, National Institute of Technology, Tiruchirappalli, 620015 Tamil Nadu; samyupsgk@gmail.com. [b]Mathematics and Basic Science, NIIT University, Neemrana, 301705 Rajasthan; G.Maradana@niituniversity.in. Translated from Prikladnaya Mekhanika i Tekhnicheskaya Fizika, Vol. 58, No. 1, pp. 132–145, January–February, 2017. Original article submitted October 24, 2014; revision submitted May 14, 2015.

 

Later, Chen [7] extended the work of Gupta and Gupta [5] to that of a nonisothermal stretching sheet. Grubka and Bobba [8] examined the heat transfer characteristics of a continuous linearly stretching surface with power-law surface temperature variation. Later, Ali [9] reported a similarity solution on a continuous stretching surface for the case of a power-law surface velocity and temperature. Moutsoglou and Chen [10] analyzed the buoyancy effects on the flow and heat transfer from an inclined continuous sheet with either a uniform wall or a uniform surface heat flux. Abdelhafez [11] and Chappidi and Gunnerson [12] examined a laminar boundary layer flow over a moving surface in a parallel free stream for two cases separately, at $U_w > U_\infty$ or $U_w < U_\infty$, and formulated two sets of boundary-value problems, while Afzal et al. [13] formulated a single set of governing equations for both problems. Considering the composite reference velocity $U(x) = U_w(x)$, Afzal and Varshney [14] investigated the flow on a continuously stretching sheet. A similarity solution of velocity fields in a laminar boundary layer driven by the stretching surface boundary was formulated by Afzal [15] for the velocity presented as $U = U_w + U_\infty$. All the above-cited studies dealt with similarity solutions. Recently, Patil et al. [16] obtained a nonsimilar solution for a mixed convection flow over a moving vertical stretching sheet in a parallel free stream. Later, Patil [17] extended the work of Patil et al. [16] to include a variable wall temperature and concentration. In that analysis, he considered uniform mass transfer (uniform suction/injection).

In many cases, mass transfer from a wall slot (slot suction/injection) into the boundary layer is of interest for various prospective applications including thermal protection, energizing the inner portion of the boundary layers with adverse pressure gradients, skin friction reduction on high-speed aircraft, etc. Finite discontinuities arise at the leading and trailing edges in the case of uniform slot suction/injection, and those can be avoided by choosing an appropriate nonuniform slot suction/injection mode. Recently, nonuniform slot suction/injection into a mixed convection boundary layer on a vertical cone was studied by Ravindran and Ganapathirao [18]. However, there are many transport processes that are governed by the simultaneous action of buoyancy forces due to the thermal and mass diffusion in the presence of the chemical reaction effect. Such processes include drying and dehydration operations in chemical and food processing plants, evaporation at the surface of water reservoirs, damage of crops due to freezing, energy transfer in a wet cooling tower, etc. Recently, the chemical reaction and heat generation/absorption effects on a mixed convection flow over a vertical wedge and vertical cone with nonuniform slot suction/injection were studied by Ganapathirao et al. [19] and Ravindran et al. [20], respectively.

As no attempt has been made to study the effects of the chemical reaction and heat generation or absorption on a mixed convection boundary layer flow over a vertical stretching sheet with nonuniform slot mass transfer, we have investigated it in this article.

## 1. MATHEMATICAL FORMULATION

Let us consider a steady mixed convection two-dimensional laminar boundary layer flow along a vertical stretching sheet moving in the vertically upward direction. The $x$ axis is taken along the vertical stretching sheet and the $y$ axis is normal to it [17]. It is assumed that both the free stream velocity $U_\infty$ and the sheet velocity $U_w$ have the same direction. The continuously stretching surface is assumed to have a power-law velocity $U_w(x) = U_{w0}x^m$ ($m$ is the velocity exponent parameter), a power-law temperature $T_w(x) = T_\infty + Bx^n$ ($T_\infty$ is the uniform ambient temperature and $B$ is a constant), and a power-law wall concentration $C_w(x) = C_\infty + B^*x^n$ ($C_\infty$ is the uniform ambient concentration, $B^*$ is a constant, and $n$ is the temperature and concentration exponent parameter). It is also assumed that the sheet surface is maintained at a variable wall temperature $T_w$ and concentration $C_w$ with $B > 0$ ($T_w > T_\infty$) corresponding to a heated sheet (assisting flow) and $B < 0$ ($T_w < T_\infty$) corresponding to a cooled sheet (opposing flow) and that $B^* > 0$ ($C_w > C_\infty$). The buoyancy force arises due to the temperature and concentration differences in the fluid. The concentrations of the diffusing species are assumed to be infinitesimally small in comparison with other chemical species far away from the sheet surface. Hence, the Soret and Dufour effects are neglected. The Boussinesq approximation is invoked for the combined heat and mass transfer problem.

Under these assumptions, the equations of conservation of mass, momentum, energy, and concentration are written as

$$\frac{\partial u}{\partial x}+\frac{\partial v}{\partial y}=0; \tag{1}$$

$$u\,\frac{\partial u}{\partial x}+v\,\frac{\partial u}{\partial y}=U_e\,\frac{\partial U_e}{\partial x}+\nu\,\frac{\partial^2 u}{\partial y^2}+g\Big[\beta(T-T_\infty)+\beta^*(C-C_\infty)\Big],$$

$$u\,\frac{\partial T}{\partial x}+v\,\frac{\partial T}{\partial y}=\frac{\nu}{\mathrm{Pr}}\,\frac{\partial^2 T}{\partial y^2}+\frac{Q_0}{\rho c_p}\,(T-T_\infty), \tag{2}$$

$$u\,\frac{\partial C}{\partial x}+v\,\frac{\partial C}{\partial y}=\frac{\nu}{\mathrm{Sc}}\,\frac{\partial^2 C}{\partial y^2}-k_1(C-C_\infty),$$

and the boundary conditions are

$$y=0: \qquad u(x,0)=U_w(x), \quad v(x,0)=v_w(x), \quad T=T_w(x), \quad C=C_w(x),$$

$$y\to\infty: \qquad u(x,\infty)\to U_\infty(x), \quad T\to T_\infty, \quad C\to C_\infty.$$

Here $u$ and $v$ are the velocity components in the $x$ and $y$ directions, $U_e$ is the composite reference velocity at the boundary layer edge, $c_p$ is the specific heat at constant pressure, $C$ is the species concentration, $C_w(x)$ is the variable concentration at the wall, $T$ is the temperature, $T_w(x)$ is the variable temperature at the wall, $g$ is the acceleration due to gravity, $k_1$ is the chemical reaction rate, Pr is the Prandtl number, $Q_0$ is the heat generation coefficient, Sc is the Schmidt number, $\nu$ is the kinematic viscosity, $\rho$ is the density of the fluid, and $\beta$ and $\beta^*$ are the volumetric coefficients of thermal and concentration expansion. The stretching sheet velocity $U_w$, free-stream velocity $U_\infty$, wall temperature $T_w$, and wall concentration $C_w$ are defined as

$$U_w(x)=U_{w0}x^m, \quad U_\infty(x)=U_{\infty0}x^m, \quad T_w(x)=T_\infty+Bx^n, \quad C_w(x)=C_\infty+B^*x^n.$$

The composite velocity is defined as

$$U(x)=U_w(x)+U_\infty(x)=U_0x^m,$$

where $U_0=U_{w0}+U_{\infty0}\neq0$. Owing to the transformations

$$\eta=y\Big(\frac{U(x)}{\nu x}\Big)^{1/2}, \qquad \xi=\Big(\frac{U(x)x}{\nu}\Big)^{1/2},$$

$$\psi(x,y)=(\nu xU(x))^{1/2}f(\xi,\eta), \qquad u=\frac{\partial\psi}{\partial y}, \qquad v=-\frac{\partial\psi}{\partial x},$$

$$u=U_0x^mF(\xi,\eta), \qquad f_\eta(\xi,\eta)=F(\xi,\eta),$$

$$v=-2^{-1}(\nu U_0)^{1/2}x^{(m-1)/2}[(m+1)(f+\xi f_\xi)+(m-1)\eta F],$$

$$T-T_\infty=(T_w-T_\infty)G(\xi,\eta), \qquad C-C_\infty=(C_w-C_\infty)H(\xi,\eta),$$

Eq. (1) is identically satisfied, and Eqs. (2) reduce to the dimensionless form

$$F_{\eta\eta}+\frac{m+1}{2}\,fF_\eta+m(\varepsilon^2-F^2)+\lambda(G+NH)=\frac{m+1}{2}\,\xi(FF_\xi-F_\eta f_\xi); \tag{3}$$

$$G_{\eta\eta}+\mathrm{Pr}\,\frac{m+1}{2}\,fG_\eta-n\mathrm{Pr}\,FG+\mathrm{Pr}\,\xi^2SG=\mathrm{Pr}\,\frac{m+1}{2}\,\xi(FG_\xi-G_\eta f_\xi); \tag{4}$$

$$H_{\eta\eta}+\mathrm{Sc}\,\frac{m+1}{2}\,fH_\eta-n\mathrm{Sc}FH-\mathrm{Sc}\xi^2\Delta H=\mathrm{Sc}\,\frac{m+1}{2}\,\xi(FH_\xi-H_\eta f_\xi), \tag{5}$$

where

$$\lambda=\frac{\mathrm{Gr}}{\mathrm{Re}_x^2}, \qquad \mathrm{Gr}=\frac{g\beta(T_w-T_\infty)x^3}{\nu^2},$$

$$\mathrm{Re}_x = \frac{U_0 x^{m+1}}{\nu}, \qquad N = \frac{\lambda^*}{\lambda}, \qquad \lambda^* = \frac{\mathrm{Gr}^*}{\mathrm{Re}_x^2}, \qquad \mathrm{Gr}^* = \frac{g\beta^*(C_w - C_\infty)x^3}{\nu^2},$$

$$\mathrm{Pr} = \frac{\nu}{\alpha}, \qquad \mathrm{Sc} = \frac{\nu}{D}, \qquad S = \frac{Q_0\nu}{U^2\rho c_p}, \qquad \Delta = \frac{k_1\nu}{U^2},$$

$\xi$ and $\eta$ are the transformed variables, $\alpha$ is the thermal diffusivity, $\Delta$ is the chemical reaction parameter, $D$ is the mass diffusivity, $f$ is the dimensionless stream function, $F$ is the dimensionless velocity in the $x$ direction, $G$ is the dimensionless temperature, $H$ is the dimensionless concentration, $S$ is the heat generation/absorption parameter, $\mathrm{Re}_x$ is the local Reynolds number, $N$ is the ratio of the buoyancy forces or of the Grashof numbers, $\lambda$ and $\lambda^*$ are the buoyancy parameters, and Gr and $\mathrm{Gr}^*$ are the local Grashof numbers due to temperature and concentration, respectively.

The mixed convection (buoyancy) parameter $\lambda > 0$ ($T_w > T_\infty$) refers to the assisting flow, $\lambda < 0$ ($T_w < T_\infty$) corresponds to the opposing flow, and $\lambda = 0$ ($T_w = T_\infty$) refers to the forced flow case. The ratio of the buoyancy forces $N$ is a dimensionless parameter representing the ratio between the thermal and concentration buoyancy forces ($N = 0$ in the case with no buoyancy effect due to mass diffusion, $N = \infty$ in the case with no buoyancy effect due to thermal diffusion, $N = 1$ for the thermal and mass buoyancy forces of the same strength, $N > 0$ for the combined buoyancy forces driving the flow, and $N < 0$ for the buoyancy forces opposing each other). The heat generation or absorption parameter is $S > 0$ in the case of heat generation, $S < 0$ in the case of hear absorption, and $S = 0$ in the case with no heat source. The chemical reaction parameter is $\Delta > 0$ in the case of species generation, $\Delta < 0$ for species consumption, and $\Delta = 0$ in the case with no chemical reaction.

The boundary conditions reduce to

$$\begin{aligned} &\eta = 0: \qquad F = 1 - \varepsilon, \quad G = 1, \quad H = 1, \\ &\eta = \eta_\infty: \qquad F = \varepsilon, \quad G = 0, \quad H = 0, \end{aligned} \tag{6}$$

where $\eta_\infty$ is the boundary layer edge and $\varepsilon$ corresponds to the ratio of free-stream velocity to the composite reference velocity:

$$\varepsilon = \frac{U_\infty(x)}{U(x)} = \frac{U_{\infty 0}}{U_{w0} + U_{\infty 0}}.$$

The similarity transformation based on the composite reference velocity $U(x)$ was first proposed by Abdelhafez [11].

The problem formulation includes the following particular cases.

1. At $\varepsilon = 1$, i.e., $U_w = 0$ (the classical Blasius flat-plate flow problem), the sheet is at rest and the fluid is in motion.

2. At $\varepsilon = 0$, i.e., $U_\infty = 0$, the fluid is at rest and the motion is created by the sheet. This case was proposed by Soundalgekar and Murty [6], and the equations for the stretching sheet were derived by Afzal and Varshney [14].

3. At $0 < \varepsilon < 1$, i.e., $U_w > 0$ and $U_\infty > 0$, both the sheet and fluid are in motion, and they are moving in the same direction.

In this article, we assume that both the stretching sheet velocity $U_w(x)$ and the free-stream velocity $U_\infty(x)$ have the same direction. The value $\varepsilon = 0.5$ throughout the computation corresponds to the parallel flow solution.

It follows from the boundary conditions that

$$f = \int_0^\eta F\, d\eta + f_w,$$

where $f$ can be written as

$$(m+1)f_w + 2(U_0/\nu)^{m/(m+1)}\xi^{2m/(m+1)}(f_\xi)_w = -(m+1)(v_w/U_0)\xi.$$

One can easily obtain

$$f_w = -\frac{2}{(m+1)U_0}\Big(\frac{U_0}{\nu}\Big)^{m/(m+1)} \int_0^\xi v_w \xi^{(1-m)/(1+m)}\, d\xi,$$

where $v_w$ is the surface mass transfer velocity with $v_w < 0$ for suction, $v_w > 0$ for injection or blowing, and $v_w = 0$ for an impermeable sheet. Here we study nonuniform single and double slot suction (injection) into a mixed convection boundary layer flow over a vertical stretching sheet.

## 2. SINGLE SLOT

In the case of a single slot, the velocity of suction (injection) is defined as

$$v_w = \begin{cases} 0, & \xi \le \xi_0, \\ -U_0 \dfrac{m+1}{2}\Big(\dfrac{\nu}{U_0}\Big)^{m/(m+1)} A\xi^{-1}\omega^* \sin\left[\omega^*(\xi-\xi_0)\right], & \xi_0 \le \xi \le \xi_0^*, \\ 0, & \xi \ge \xi_0^*. \end{cases}$$

Then, the expression for the function $f_w$ turns to

$$f_w = \begin{cases} 0, & \xi \le \xi_0, \\ A\xi^{-1}\{1-\cos\left[\omega^*(\xi-\xi_0)\right]\}, & \xi_0 \le \xi \le \xi_0^*, \\ A\xi^{-1}\{1-\cos\left[\omega^*(\xi_0^*-\xi_0)\right]\}, & \xi \ge \xi_0^*. \end{cases}$$

Here $\omega^*$ and $\xi_0$ are the free parameters that determine the slot length and slot location, respectively. The function $v_w$ is continuous for all values of $\xi$ and has nonzero values only in the interval $[\xi_0, \xi_0^*]$.

## 3. DOUBLE SLOT

In the case of a double slot, $v_w$ is taken as

$$v_w = \begin{cases} 0, & \xi \le \xi_1, \\ -U_0 \dfrac{m+1}{2}\Big(\dfrac{\nu}{U_0}\Big)^{m/(m+1)} A\xi^{-1}\omega^* \sin\left[\omega^*(\xi-\xi_1)\right], & \xi_1 \le \xi \le \xi_1^*, \\ 0, & \xi_1^* \le \xi \le \xi_2, \\ -U_0 \dfrac{m+1}{2}\Big(\dfrac{\nu}{U_0}\Big)^{m/(m+1)} A\xi^{-1}\omega^* \sin\left[\omega^*(\xi-\xi_2)\right], & \xi_2 \le \xi \le \xi_2^*, \\ 0, & \xi \ge \xi_2^*. \end{cases}$$

Using $v_w$, we can express $f_w$ as

$$f_w = \begin{cases} 0, & \xi \le \xi_1, \\ A\xi^{-1}\{1-\cos\left[\omega^*(\xi-\xi_1)\right]\}, & \xi_1 \le \xi \le \xi_1^*, \\ A\xi^{-1}\{1-\cos\left[\omega^*(\xi_1^*-\xi_1)\right]\}, & \xi_1^* \le \xi \le \xi_2, \\ A\xi^{-1}\{1-\cos\left[\omega^*(\xi_1^*-\xi_1)\right]\} + A\xi^{-1}\{1-\cos\left[\omega^*(\xi-\xi_2)\right]\}, & \xi_2 \le \xi \le \xi_2^*, \\ A\xi^{-1}\{1-\cos\left[\omega^*(\xi_1^*-\xi_1)\right]\} + A\xi^{-1}\{1-\cos\left[\omega^*(\xi_2^*-\xi_2)\right]\}, & \xi \ge \xi_2^*. \end{cases}$$

Here $\xi_1$ and $\xi_2$ are the parameters that determine the starting points of the first and second slot locations, respectively. Hence, the continuous function $v_w$ has nonzero values only in the intervals $[\xi_1, \xi_1^*]$ and $[\xi_2, \xi_2^*]$.

The main physical quantities of interest are the local skin friction coefficient $C_{fx}$, local Nusselt number $\mathrm{Nu}_x$, and local Sherwood number $\mathrm{Sh}_x$, which represent the wall shear stress, heat transfer rate, and mass transfer rate, respectively.

The local skin friction coefficient at the wall can be expressed as

$$C_{fx} = \frac{2}{\rho U^2}\left[\mu\,\frac{\partial u}{\partial y}\right]\Big|_{y=0},$$

or

$$C_{fx}(\mathrm{Re}_x)^{1/2} = 2F_\eta(\xi, 0).$$

The heat transfer coefficient at the wall can be expressed in terms of the local Nusselt number as

$$\mathrm{Nu}_x = -\frac{1}{T_w - T_\infty}\left[x\,\frac{\partial T}{\partial y}\right]\Big|_{y=0},$$

or

$$\mathrm{Nu}_x(\mathrm{Re}_x)^{-1/2} = -G_\eta(\xi, 0),$$

and the mass transfer coefficient at the wall can be expressed in terms of the local Sherwood number as

$$\mathrm{Sh}_x = -\frac{1}{C_w - C_\infty}\left[x\,\frac{\partial C}{\partial y}\right]\Big|_{y=0},$$

or

$$\mathrm{Sh}_x(\mathrm{Re}_x)^{-1/2} = -H_\eta(\xi, 0).$$

## 4. METHOD OF THE SOLUTION

The set of coupled nonlinear partial differential equations (3)–(5) along with the boundary conditions (6) represent a two-point boundary-value problem for partial differential equations, which are solved numerically by using an implicit finite difference scheme combined with the quasi-linearization technique [18, 20, 23, 24].

Applying the quasi-linearization technique, we replace the nonlinear coupled partial differential equations (3)–(5) by the following system of linear partial differential equations:

$$F_{\eta\eta}^{i+1} + X_1^i F_\eta^{i+1} + X_2^i F^{i+1} + X_3^i G^{i+1} + X_4^i F_\xi^{i+1} + X_5^i H^{i+1} = X_6^i,$$

$$G_{\eta\eta}^{i+1} + Y_1^i G_\eta^{i+1} + Y_2^i G^{i+1} + Y_3^i F^{i+1} + Y_4^i G_\xi^{i+1} = Y_5^i, \tag{7}$$

$$H_{\eta\eta}^{i+1} + Z_1^i H_\eta^{i+1} + Z_2^i H^{i+1} + Z_3^i F^{i+1} + Z_4^i H_\xi^{i+1} = Z_5^i.$$

The coefficient functions with the iterative index $i$ are known, and the functions with the iterative index $i+1$ are to be determined.

After quasi-linearization, the boundary conditions become

$$\eta = 0: \qquad F^{i+1} = 1 - \varepsilon, \quad G^{i+1} = 1, \quad H^{i+1} = 1,$$

$$\eta = \eta_\infty: \qquad F^{i+1} = \varepsilon, \quad G^{i+1} = 0, \quad H^{i+1} = 0.$$

The coefficients in Eqs. (7) are defined as

$$X_1^i = f\,\frac{m+1}{2} + \frac{m+1}{2}\,\xi f_\xi, \quad X_2^i = -2mF - \frac{m+1}{2}\,\xi F_\xi, \quad X_3^i = \lambda,$$

$$X_4^i = -\frac{m+1}{2}\,\xi F, \quad X_5^i = N\lambda, \quad X_6^i = -\frac{m+1}{2}\,\xi F F_\xi - m(\varepsilon^2 + F^2),$$

$$Y_1^i = \mathrm{Pr}\left(\frac{m+1}{2}\,f + \frac{m+1}{2}\,\xi f_\xi\right), \quad Y_2^i = \mathrm{Pr}\,(S\xi^2 - nF), \quad Y_3^i = -\mathrm{Pr}\left(\frac{m+1}{2}\,\xi G_\xi + nG\right),$$

$$Y_4^i = -\mathrm{Pr}\,\frac{m+1}{2}\,\xi F, \qquad Y_5^i = -\mathrm{Pr}\left(\frac{m+1}{2}\,\xi F G_\xi + nFG\right),$$

$$Z_1^i = \mathrm{Sc}\left(\frac{m+1}{2}\,f + \frac{m+1}{2}\,\xi f_\xi\right), \quad Z_2^i = -\mathrm{Sc}\,(\Delta\xi^2 + nF), \quad Z_3^i = -\mathrm{Sc}\left(\frac{m+1}{2}\,\xi H_\xi + nH\right),$$

$$Z_4^i = -\mathrm{Sc}\,\frac{m+1}{2}\,\xi F, \qquad Z_5^i = -\mathrm{Sc}\left(\frac{m+1}{2}\,\xi F H_\xi + nFH\right).$$

The resulting system of linear algebraic equations with a block tridiagonal matrix is solved by using Varga's algorithm [24].

The step sizes in the $\xi$ and $\eta$ directions are chosen as $\Delta\xi = 0.005$ and $\Delta\eta = 0.01$. A convergence criterion based on the relative difference between the current and previous iteration values is employed:

$$\max\left\{|(F_\eta)_w^{i+1} - (F_\eta)_w^i|, |(G_\eta)_w^{i+1} - (G_\eta)_w^i|, |(H_\eta)_w^{i+1} - (H_\eta)_w^i|\right\} < 10^{-5}.$$

**Table 1.** Comparison of the heat transfer rates $-G_\eta(\xi,0)$ for $\lambda=0$, $\xi=0$, $\varepsilon=0$, $m=0$, $n=0$, $N=0$, $S=0$, $\Delta=0$, Sc $=0$, $A=0$, and different values of Pr

| Pr | $-G_\eta(\xi,0)$ | | | | | | | |
|---|---|---|---|---|---|---|---|---|
| | Data [2] | Data [6] | Data [7] | Data [9] | Data [10] | Data [16] | Data [17] | Present work |
| 0.7 | 0.3492 | 0.3508 | 0.34925 | 0.3476 | 0.34924 | 0.35004 | 0.352215 | 0.3542 |
| 1.0 | 0.4438 | — | 0.44375 | 0.4416 | — | 0.44401 | 0.444428 | 0.4445 |
| 2.0 | — | 0.6831 | 0.68324 | — | — | 0.68314 | 0.683024 | 0.6830 |
| 7.0 | — | — | 1.38619 | — | 1.38703 | 1.38625 | 1.386861 | 1.3869 |
| 10.0 | 1.6804 | 1.6808 | 1.68008 | 1.6713 | — | 1.68011 | 1.680150 | 1.6802 |
| 100.0 | 5.5450 | — | 5.54400 | — | — | 5.54610 | 5.547512 | 5.5475 |

**Table 2.** Comparison of the heat transfer rates $-G_\eta(\xi,0)$ for $m=1$, $\lambda=0$, $\xi=0$, $\varepsilon=0$, $N=0$, $S=0$, $\Delta=0$, Sc $=0$, $A=0$, and different values of Pr and $n$

| Pr | $-G_\eta(\xi,0)$ | | | | | | | | |
|---|---|---|---|---|---|---|---|---|---|
| | Present work | | | Data [7] | | | Data [8] | | |
| | $n=-2$ | $n=0$ | $n=2$ | $n=-2$ | $n=0$ | $n=2$ | $n=-2$ | $n=0$ | $n=2$ |
| 0.72 | −0.7202 | 0.4637 | 1.0902 | 53 | −0.72 | 0.4631 | 1.0855 | | |
| 1.00 | −0.9959 | 0.5821 | 1.3333 | −1.00003 | 0.58199 | 1.33334 | −1.00 | 0.5820 | 1.3333 |
| 3.00 | −2.9995 | 1.1654 | 2.5097 | −3.00046 | 1.16523 | 2.50972 | −3.00 | 1.1652 | 2.5097 |
| 7.00 | −7.0026 | 1.8955 | 3.9716 | −7.00240 | 1.89537 | 3.97150 | — | — | — |
| 10.00 | −9.9963 | 2.3083 | 4.7969 | −10.00470 | 2.30796 | 4.79686 | −10.00 | 2.3080 | 4.7969 |
| 100.00 | −100.2990 | 7.7745 | 15.7124 | −100.31000 | 7.76536 | 15.71180 | −100.00 | 7.7657 | 15.7120 |

## 5. RESULTS AND DISCUSSION

The computations were carried out for $0.7 \le \text{Pr} \le 100.0$, $-0.5 \le A \le 1.0$, $-0.5 \le \lambda \le 7.0$, $-1.0 \le S \le 1.0$, $-5.0 \le \Delta \le 3.0$, $0.22 \le \text{Sc} \le 0.60$, $0 \le m \le 1.0$, $-2.0 \le n \le 2.0$, $N = 0.5$, and $\varepsilon = 0.5$. In all the numerical computations, the edge of the boundary layer was taken in the interval $4 \leqslant \eta_\infty \leqslant 8$, depending upon the values of the parameters. In order to verify the accuracy of the present numerical approach, we compared the results of the surface heat transfer parameter $-G_\eta(\xi,0)$, velocity $F$, and temperature $G$ profiles with the results previously published by Tsou et al. [2], Soundalgekar and Murty [6], Chen [7], Grubka and Bobba [8], Ali [9], Moutsoglou and Chen [10], Afzal [15], Patil et al. [16], and Patil [17]. The results are found to be in very good agreement and some of the comparisons are shown in Tables 1 and 2 and in Figs. 1 and 2. It is noticed from Table 1 that the surface heat transfer parameter $-G_\eta(\xi,0)$ increases significantly with Pr as the higher Prandtl number fluid has a smaller thermal boundary layer thickness. It is observed from Table 2 that an increase in the temperature exponent parameter $n$ causes an increase in the negative temperature gradient.

The velocity profiles $F$ are shown in Fig. 1. The results indicate that there is a gradual variation in the velocity profile as the parameter $\varepsilon$ increases from 0 to 1. The effect of the temperature exponent parameter $n$ on the temperature profiles $G$ is illustrated in Fig. 2. The results shows that an increase in $n$ causes a decrease in the thermal boundary layer thickness.

The effects of the buoyancy parameter $\lambda$ and Prandtl number Pr on the velocity $F$ and temperature $G$ profiles are shown in Fig 3. Both the assisting flow ($\lambda > 0$) and opposing flow ($\lambda < 0$) cases are considered here. We observe that the overshoot occurs in the velocity profiles $F$ for the buoyancy assisting flow ($\lambda > 0$) near the wall of the stretching sheet for the lower Prandtl number fluid with Pr $= 0.7$ (air). The buoyancy assisting flow ($\lambda > 0$) acts as a favorable pressure gradient resulting in an increase in velocity. The buoyancy opposing flow ($\lambda < 0$) gives rise to an adverse pressure gradient, which reduces the flow velocity. The effect of $\lambda$ on the temperature profiles is comparatively less pronounced, which can be seen in Fig. 3b. Moreover, it is observed from Fig. 3b that the high Prandtl number result in a thinner thermal boundary layer as the higher Prandtl number fluid with Pr $= 7.0$ (water) has a lower thermal conductivity.

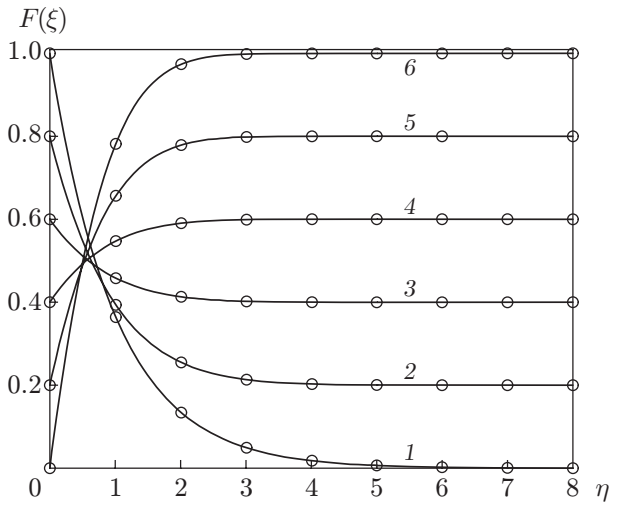


**Fig. 1.**

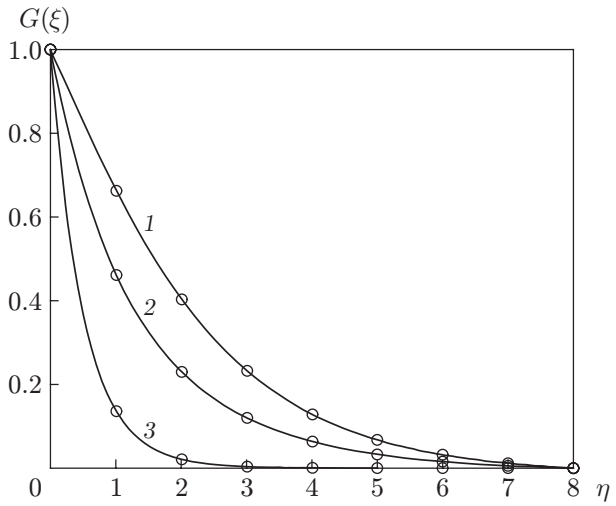


**Fig. 2.**

**Fig. 1.** Velocity versus the coordinate $\eta$ for $\lambda = 0$, $n = 1.0$, $\xi = 0$, $A = 0$, $m = 1.0$, $N = 0$, $S = 0$, Sc $= 0$, Pr $= 0$, $\Delta = 0$, and different values of $\varepsilon$: the curves and points are the data of the present work and those of [15], respectively; $\varepsilon = 0$ (*1*), 0.2 (*2*), 0.4 (*3*), 0.6 (*4*), 0.8 (*5*), and 1.0 (*6*).

**Fig. 2.** Temperature versus the coordinate $\eta$ for $\lambda = 0$, $\varepsilon = 0$, $\xi = 0$, $A = 0$, $m = 0$, $N = 0$, $S = 0$, Sc $= 0$, Pr $= 0.7$, $\Delta = 0$, and different values of the temperature exponent parameter $n$: the curves and points are the data of the present work and those of [6], respectively; $n = 0$ (*1*), 1 (*2*), and 2 (*3*).

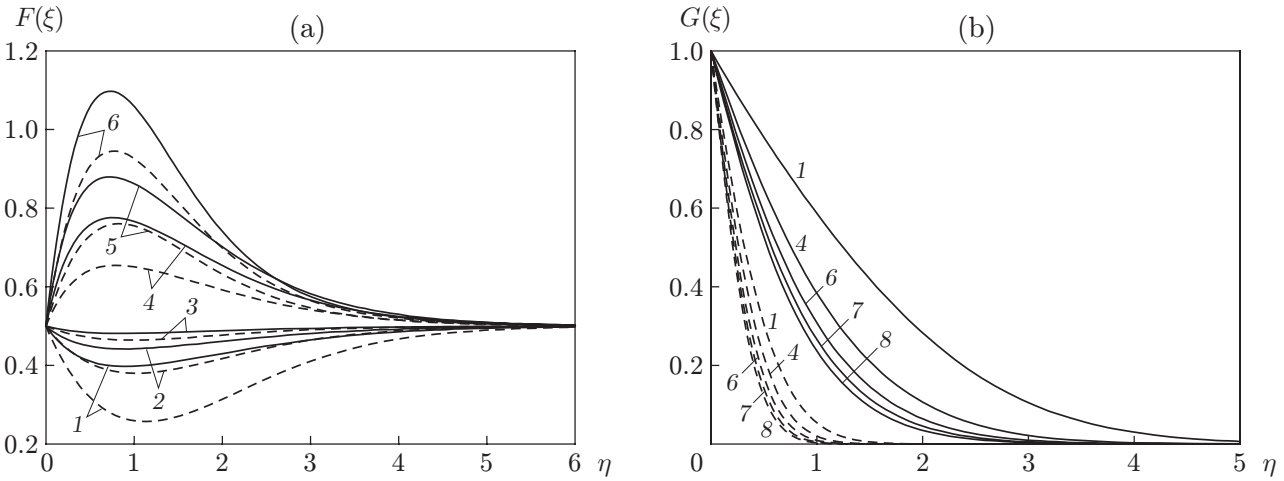


**Fig. 3.** Velocity (a) and temperature (b) profiles versus the coordinate $\eta$ for $\varepsilon = 0.5$, $\omega^* = 2\pi$, $S = 0.5$, $N = 0.5$, $m = 1.0$, $n = 1.0$, $A = 0.5$, $\Delta = 0.5$, Sc $= 0.22$, $\xi = 0.75$, and different values of the buoyancy parameter $\lambda$ and Prandtl number Pr: the solid and dashed curves refers to Pr $= 0.7$ and 7.0, respectively; $\lambda = -0.5$ (*1*), $-0.3$ (*2*), $-0.1$ (*3*), 1.0 (*4*), 2.0 (*5*), 3.0 (*6*), 5.0 (*7*), and 7.0 (*8*).

Figure 4 depicts the effect of the surface mass transfer parameter $A$ and the temperature exponent parameter $n$ on the temperature profiles $G$. Injection ($A < 0$) causes a decrease in the steepness of the temperature profiles near the wall of the stretching sheet within the boundary layer, but the steepness of the temperature profiles increases in the case with suction ($A > 0$). It is also observed that the thermal boundary layer thickness decreases with the linearly stretching surface temperature ($n = 1$) and increases with the uniform surface temperature ($n = 0$).

The effects of the surface mass transfer parameter $A$ and the velocity exponent parameter $m$ on the velocity profiles $F$ are shown in Fig. 5. It is observed that the velocity increases in the case of the linearly stretching surface ($m = 1$) and decreases in the case of uniform motion ($m = 0$). The effect of $m$ on the temperature $G$ and concentration $H$ profiles is very small.

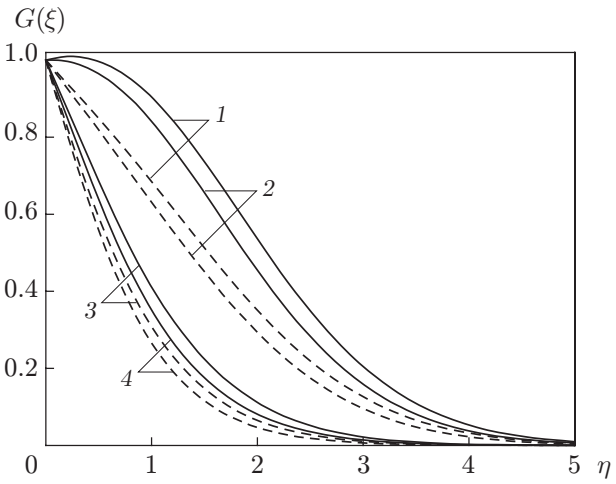


**Fig. 4.**

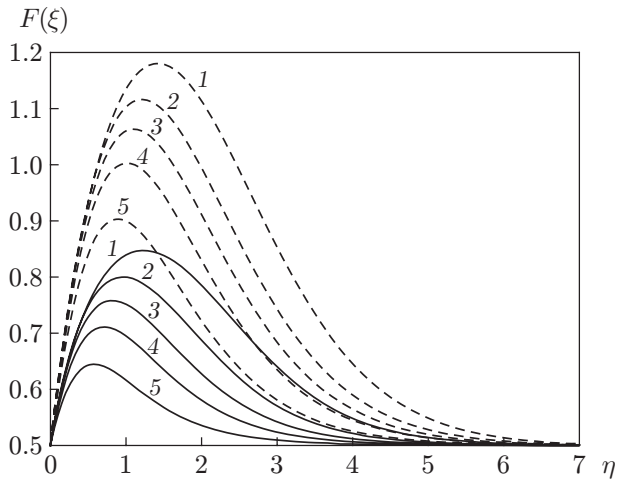


**Fig. 5.**

**Fig. 4.** Temperature versus the coordinate $\eta$ for $\varepsilon = 0.5$, $S = 0.5$, $N = 0.5$, $m = 1.0$, $\lambda = 1.0$, Pr $= 0.7$, $\Delta = 0.5$, Sc $= 0.22$, $\xi = 1.0$, and $\omega^* = 2\pi$ for the slot position with the boundaries at $\xi_0 = 0.5$ and $\xi_0^* = 1.0$: the solid and dashed curves refer to $n = 0$ and 1, respectively; $A = -0.5$ (*1*), $-0.4$ (*2*), 0 (*3*), and 0.3 (*4*).

**Fig. 5.** Velocity versus the coordinate $\eta$ for $\varepsilon = 0.5$, $S = 0.5$, $N = 0.5$, $n = 1.0$, $\lambda = 1.0$, Pr $= 0.7$, $\Delta = 1.0$, Sc $= 0.22$, $\xi = 1.0$, and $\omega^* = 2\pi$ for the slot position with the boundaries at $\xi_0 = 0.5$ and $\xi_0^* = 1.0$: the solid and dashed curves refer to $m = 0$ and 1, respectively; $A = -0.5$ (*1*), $-0.2$ (*2*), 0 (*3*), 0.2 (*4*), and 0.5 (*5*).

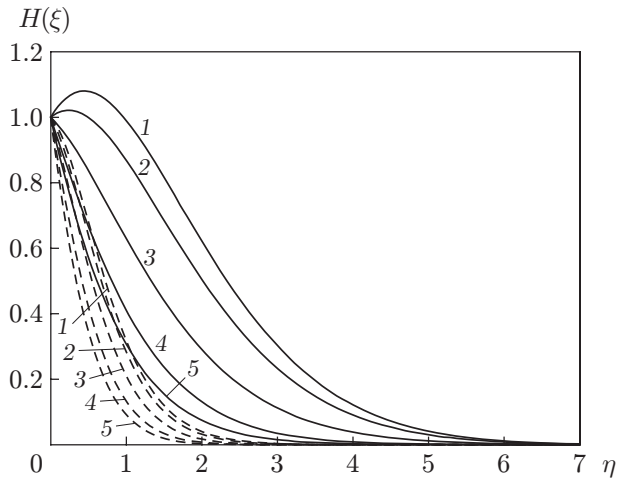


**Fig. 6.** Concentration versus the coordinate $\eta$ for $\varepsilon = 0.5$, $\omega^* = 2\pi$, $S = 0.5$, $N = 0.5$, $n = 1.0$, $\lambda = 1.0$, Pr $= 0.7$, $m = 1.0$, $A = 1.0$, $\xi = 1.0$, and different values of the Schmidt number Sc and chemical reaction parameter $\Delta$: the solid and dashed curves refer to Sc $= 0.22$ and 0.60, respectively; $\Delta = -5.0$ (*1*), $-4.5$ (*2*), $-3.0$ (*3*), 0 (*4*), and 3.0 (*5*).

Figure 6 displays the effects of the chemical reaction parameter $\Delta$ and the Schmidt number Sc on the concentration profiles $H$. The concentration boundary layer thickness increases at $\Delta < 0$ and decreases at $\Delta > 0$. The values of the Schmidt number are chosen to be realistic, representing diffusing chemical species of most common interest: hydrogen (Sc $= 0.22$) and water vapour (Sc $= 0.60$) at $T = 25°$C and atmospheric pressure $p = 10^5$ Pa. It is evident that an increase in Sc causes a decrease in the concentration boundary layer thickness. The physical reason is that the higher values of Sc correspond to low mass diffusivity. The effect of Sc on the velocity $F$ and temperature $G$ profiles is very small because this physical parameter appears only in the concentration equation.

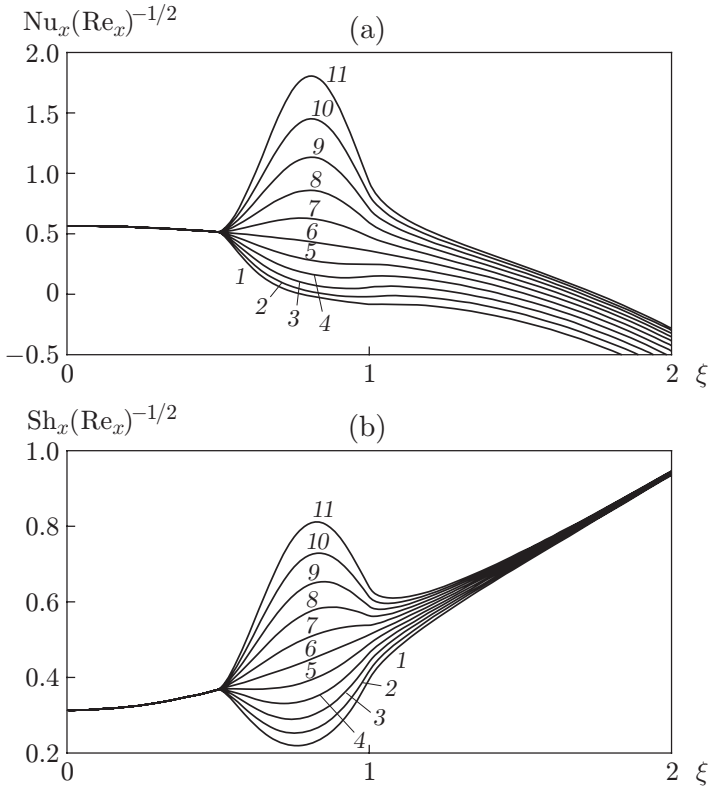


**Fig. 7.** Local Nusselt number $\mathrm{Nu}_x(\mathrm{Re}_x)^{-1/2}$ (a) and Sherwood number $\mathrm{Sh}_x(\mathrm{Re}_x)^{-1/2}$ (b) versus the coordinate $\xi$ for $\mathrm{Pr} = 0.7$, $\lambda = 1.0$, $S = 0.5$, $N = 0.5$, $m = 1.0$, $n = 1.0$, $\varepsilon = 0.5$, $\Delta = 1.0$, $\mathrm{Sc} = 0.22$, and $\omega^* = 2\pi$ for the slot location with the boundaries at $\xi_0 = 0.5$ and $\xi_0^* = 1.0$: $A = -0.5$ (*1*), $-0.4$ (*2*), $-0.3$ (*3*), $-0.2$ (*4*), $-0.1$ (*5*), 0 (*6*), 0.1 (*7*), 0.2 (*8*), 0.3 (*9*), 0.4 (*10*), and 0.5 (*11*).

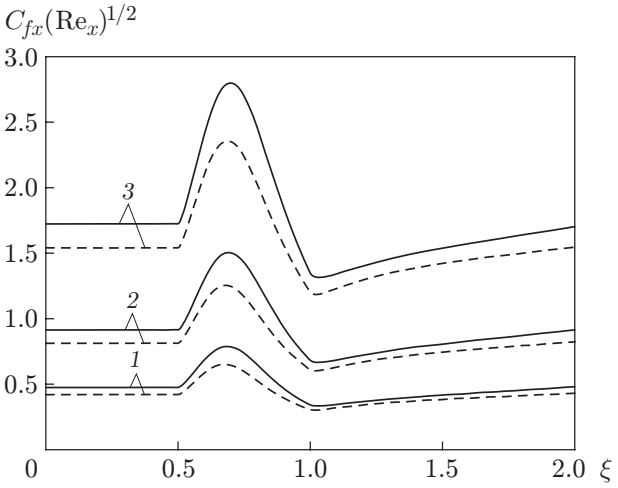


**Fig. 8.**

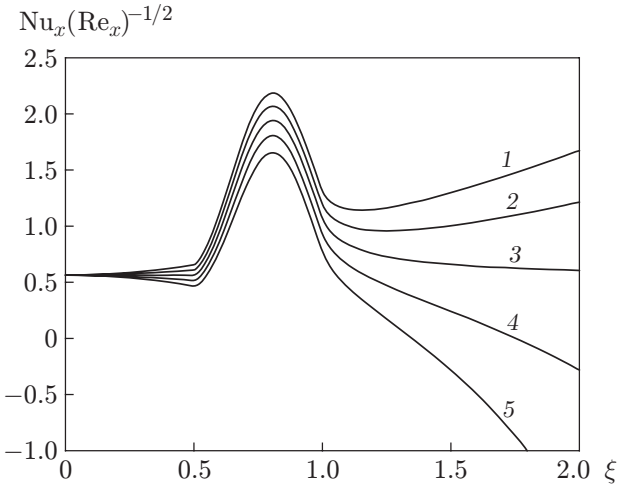


**Fig. 9.**

**Fig. 8.** Local skin friction coefficient $C_{fx}(\mathrm{Re}_x)^{1/2}$ versus the coordinate $\xi$ for $\mathrm{Pr} = 0.7$, $A = 0.5$, $S = 0.5$, $N = 0.5$, $m = 1.0$, $\varepsilon = 0.5$, $\Delta = 1.0$, $\mathrm{Sc} = 0.22$, and $\omega^* = 2\pi$ for the slot location with the boundaries at $\xi_0 = 0.5$ and $\xi_0^* = 1.0$: the solid and dashed curves refer to $n = 0$ and 1, respectively; $\lambda = 0.25$ (*1*), 0.5 (*2*), and 1.0 (*3*).

**Fig. 9.** Local Nusselt number $\mathrm{Nu}_x(\mathrm{Re}_x)^{-1/2}$ versus the coordinate $\xi$ for $\lambda = 1.0$, $A = 0.5$, $\Delta = 1.0$, $N = 0.5$, $m = 1.0$, $n = 1.0$, $\varepsilon = 0.5$, $\mathrm{Pr} = 0.7$, $\mathrm{Sc} = 0.22$, and $\omega^* = 2\pi$ for the slot location with the boundaries at $\xi_0 = 0.5$ and $\xi_0^* = 1.0$: $S = -1.0$ (*1*), $-0.5$ (*2*), 0 (*3*), 0.5 (*4*), and 1.0 (*5*).

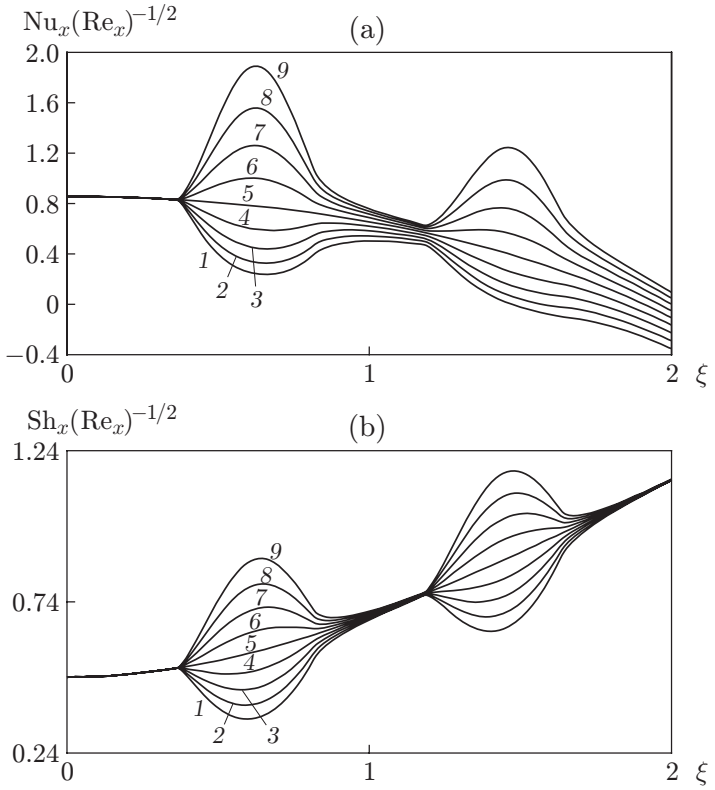


**Fig. 10.** Local Nusselt number $\mathrm{Nu}_x(\mathrm{Re}_x)^{-1/2}$ (a) and Sherwood number $\mathrm{Sh}_x(\mathrm{Re}_x)^{-1/2}$ (b) versus the coordinate $\xi$ for $\lambda = 1.0$, $\mathrm{Sc} = 0.22$, $n = 1.0$, $S = 0.5$, $N = 0.5$, $m = 1.0$, $\varepsilon = 0.5$, $\mathrm{Pr} = 0.7$, $\Delta = 1.0$, and $\omega^* = 2\pi$ for the double slot with the boundaries at $\xi_1 = 0.4$, $\xi_1^* = 0.9$ and $\xi_2 = 1.3$, $\xi_2^* = 1.8$: $A = -0.4$ (*1*), $-0.3$ (*2*), $-0.2$ (*3*), $-0.1$ (*4*), 0 (*5*), 0.1 (*6*), 0.2 (*7*), 0.3 (*8*), and 0.4 (*9*).

Figure 7 shows the effect of nonuniform suction ($A > 0$) and injection ($A < 0$) of a single slot located at $\xi_0 = 0.5$ on the local Nusselt number $\mathrm{Nu}_x(\mathrm{Re}_x)^{-1/2}$ and Sherwood numbers $\mathrm{Sh}_x(\mathrm{Re}_x)^{-1/2}$. In the case of nonuniform slot suction ($A > 0$), the local Nusselt and Sherwood numbers gradually increase from the leading edge of the slot, attain their maximum values, and then start decreasing at the rear end of the slot. Nonuniform slot injection produces the reverse effect.

Figure 8 illustrates the effects of the buoyancy parameter $\lambda$ and the temperature exponent parameter $n$ on the local skin friction coefficient $C_{fx}(\mathrm{Re}_x)^{1/2}$. The local skin friction coefficient enhances with the buoyancy parameter. The physical reason is that the buoyancy assisting flow $\lambda > 0$ implies a favorable pressure gradient, and the fluid gets accelerated, which results in a thinner momentum boundary layer and, hence, a higher skin friction coefficient at the wall. In particular, for $\lambda = 1$ and $\xi = 0.7$, the skin friction coefficient increases approximately by 19%.

Figure 9 displays the effect of the heat generation or absorption parameter $S$ on the local Nusselt number $\mathrm{Nu}_x(\mathrm{Re}_x)^{-1/2}$. It is evident that the local Nusselt number decreases with heat generation ($S > 0$) and increases with heat absorption ($S < 0$). The physical reason is that the presence of heat generation ($S > 0$) has the tendency to increase the thermal state of the fluid causing its temperature and thermal boundary layer thickness to increase; consequently, the heat transfer rate decreases. At $S = 0.5$ and 1.0, the heat transfer rate becomes negative. In the case of heat absorption ($S < 0$) both the fluid temperature and its thermal boundary layer thickness tend to decrease; consequently, the heat transfer rate increases.

Figure 10 reveals the effects of nonuniform double slot suction/injection on the local Nusselt number $\mathrm{Nu}_x(\mathrm{Re}_x)^{-1/2}$ and Sherwood number $\mathrm{Sh}_x(\mathrm{Re}_x)^{-1/2}$. In the double slot suction, the local Nusselt and Sherwood numbers increase near the first and second slots. In the case of nonuniform double slot injection, these parameters decrease near the slots.

## CONCLUSIONS

The problem of a steady mixed convection boundary layer flow over a vertical stretching sheet in the presence of the chemical reaction, and heat generation or absorption with nonuniform slot mass transfer is studied in the present paper. From the numerical results, it is observed that the buoyancy force produces a remarkable overshoot near the surface within the boundary layer for the lower Prandtl number fluid (Pr $= 0.7$) than for the higher Prandtl number fluid. It is also observed that an increase in the suction parameter effect is manifested as a decrease in the flow velocity. It is also found that the boundary layer is thinner in the case of suction, whereas the wall shear stress, heat transfer rate, and mass transfer rate are greater than in the case of injection. In particular, as the suction parameter increases from 0 to 0.4, the heat transfer and mass transfer rates are enhanced approximately by 15 and 30%, respectively. The concentration distribution increases at the chemical reaction parameter $\Delta < 0$ and decreases at $\Delta > 0$. The presence of heat generation ($S > 0$) causes an increase in the thermal boundary layer thickness, while heat absorption ($S < 0$) has the tendency to reduce the fluid temperature and the thermal boundary layer thickness.

## REFERENCES


1. B. C. Sakiadis, "Boundary Layer Behavior on Continuous Solid Surfaces. 2. The Boundary Layer on a Continuous Flat Surface," AIChE J. **7** (2), 221–225 (1961).
2. F. K. Tsou, E. M. Sparrow, and R. J. Goldstein, "Flow and Heat Transfer in the Boundary Layer on a Continuous Moving Surface," Int. J. Heat Mass Transfer **10** (2), 219–235 (1967).
3. L. E. Erickson, L. T. Fan, and V. G. Fox, "Heat and Mass Transfer on Moving Continuous Flat Plate with Suction or Injection," Industr. Eng. Chem. Fund. **5** (1), 19–25 (1966).
4. L. J. Crane, "Flows Past a Stretching Plate," Z. Angew. Math. Phys. **21** (4), 645–647 (1970).
5. P. S. Gupta and A. S. Gupta, "Heat and Mass Transfer on a Stretching Sheet with Suction or Blowing," Canad. J. Chem. Eng. **55** (6), 744–746 (1977).
6. V. M. Soundalgekar and T. V. R. Murty, "Heat Transfer in Flow Past a Continuous Moving Plate with Variable Temperature," Wärme- und Stoffübertrag **14** (2), 91–93 (1980).
7. C. H. Chen, "Heat Transfer Characteristics of a Non Isothermal Surface Moving Parallel to a Free Stream," Acta Mech. **142** (1–4), 195–205 (2000).
8. L. T. Grubka and K. M. Bobba, "Heat Transfer Characteristics of a Continuous Stretching Surface with Variable Temperature," Trans. ASME, J. Heat Transfer **107**, 248–250 (1985).
9. M. E. Ali, "Heat Transfer Characteristics of a Continuous Stretching Surface," Wärme- und Stoffübertrag **29** (4), 227–234 (1994).
10. A. Moutsoglou and T. S. Chen, "Buoyancy Effects in Boundary Layers on Inclined, Continuous, Moving Sheets," Trans. ASME, J. Heat Transfer **102** (1), 371–373 (1980).
11. T. A. Abdelhafez, "Skin Friction and Heat Transfer on a Continuous Flat Surface Moving in a Parallel Free Stream," Int. J. Heat Mass Transfer **28** (6), 1234–1237 (1985).
12. P. R. Chappidi and F. S. Gunnerson, "Analysis of Heat and Momentum Transport along a Moving Surface," Int. J. Heat Mass Transfer **32** (7), 1383–1386 (1989).
13. N. Afzal, A. Baderuddin, and A. A. Elgarvi, "Momentum and Heat Transport on a Continuous Flat Surface Moving in a Parallel Stream," Int. J. Heat Mass Transfer **36** (13), 3399–3403 (1993).
14. N. Afzal and I. S. Varshney, "The Cooling of a Low Heat Resistance Sheet Moving through a Fluid," Wärme- und Stoffübertrag **14** (4), 289–293 (1980).
15. N. Afzal, "Momentum Transfer on Power Law Stretching Plate with Free Stream Pressure Gradient," Int. J. Eng. Sci **41** (11) 1197–1207 (2003).
16. P. M. Patil, S. Roy, and A. J. Chamkha, "Mixed Convection Flow over a Vertical Power Law Stretching Sheet," Int. J. Numer. Methods Heat Fluid Flow **20** (4), 445–458 (2010).
17. P. M. Patil, "Effects of Surface Mass Transfer on Steady Mixed Convection Flow from Vertical Stretching Sheet with Variable Wall Temperature and Concentration," Int. J. Numer. Methods Heat Fluid Flow **22** (3), 287–305 (2012).
18. R. Ravindran and M. Ganapathirao, "Non-Uniform Slot Suction/Injection into Mixed Convection Boundary Layer Flow over Vertical Cone," Appl. Math. Mech. **34** (11), 1327–1338 (2013).

19. M. Ganapathirao, R. Ravindran, and I. Pop, "Non-Uniform Slot Suction (Injection) on an Unsteady Mixed Convection Flow over a Wedge with Chemical Reaction and Heat Generation," Int. J. Heat Mass Transfer **67**, 1054–1061 (2013).
20. R. Ravindran, M. Ganapathirao, and I. Pop, "Effects of Chemical Reaction and Heat Generation/Absorption on Unsteady Mixed Convection MHD Flow over a Vertical Cone with Non-Uniform Slot Mass Transfer," Int. J. Heat Mass Transfer **73**, 743–751 (2014).
21. H. S. Schlichting, *Boundary Layer Theory*, Ed. by H. S. Schlichting, and K. Gersten (Springer, New York, 2000).
22. K. Inouye and A. Tate, "Finite Difference Version Quasi-Linearization Applied to Boundary Layer Equations," AIAA J. **12**, 558–560 (1974).
23. M. Ganapathirao, R. Ravindran, and M. Momoniat, "Effects of Chemical Reaction, Heat and Mass Transfer on an Unsteady Mixed Convection Boundary Layer Flow over a Wedge with Heat Generation/Absorption in the Presence of Suction or Injection," Heat Mass Transfer **51** (2), 289–300 (2014).
24. R. S. Varga, *Matrix Iterative Analysis* (Springer, New York, 2000).